White *et al. Microstructures* 2024;4:2024050
DOI: 10.20517/microstructures.2024.26

Microstructures

Research Article

Open Access

A theoretical investigation on sulfidated nanoscale zero valent iron for removal of cis-DCE and PCE

Jessica Jein White[1], Ming Zhou[1], Jack Jon Hinsch[1], William W. Bennett[2], Yun Wang[1]

[1]Centre for Catalysis and Clean Energy, School of Environment and Science, Griffith University, Gold Coast Campus, Southport, Queensland 4222, Australia.
[2]Coastal and Marine Research Centre, Cities Research Institute, Griffith University, Gold Coast Campus, Queensland 4222, Australia.

Correspondence to: Prof. Yun Wang, Centre for Catalysis and Clean Energy, School of Environment and Science, Griffith University, Gold Coast Campus, 1 Parklands Drive, Southport, Queensland 4222, Australia. E-mail: yun.wang@griffith.edu.au

How to cite this article: White JJ, Zhou M, Hinsch JJ, Bennett WW, Wang Y. A theoretical investigation on sulfidated nanoscale zero valent iron for removal of cis-DCE and PCE. *Microstructures* 2024;4:2024050. https://dx.doi.org/10.20517/microstructures.2024.26

Received: 19 Mar 2024 **First Decision:** 18 Apr 2024 **Revised:** 3 May 2024 **Accepted:** 17 Jul 2024 **Published:** 10 Aug 2024

Academic Editors: Zhigang Chen, Liangzhi Kou **Copy Editor:** Fangling Lan **Production Editor:** Fangling Lan

Abstract

The organochlorine contaminants in wastewater can be degraded by using sulfidated nanoscale zero-valent iron. However, the specific role of S dopants and the underlying degradation mechanism are largely unknown. In this study, we applied ab initio molecular dynamics and density functional theory to investigate the remediation mechanism of two chlorinated organic compounds, cis-dichloroethene and tetrachloroethene, focusing on the role of sulfur dopant coverage on the nZVI surface, represented by a stepped Fe(211) facet, and compare it to a flat (110) surface. Our results revealed that low S coverage facilitates the dissociation of the contaminants due to stronger interaction with the iron surface. Conversely, high S coverage initially hinders dissociation but promotes adsorption of the contaminants for later dissociation, suggesting a potential benefit for remediation. By comparing with the water molecule adsorption energies, we demonstrate that S doping enhances selectivity towards these contaminants only at high S coverage. Our theoretical findings, therefore, highlight the importance of optimizing S coverage for effective wastewater treatment using sulfidated nanoscale zero-valent iron.

Keywords: Nanoscale zero-valent iron, sulfidation, stepped surfaces, hydrophobicity, density functional theory, *ab initio* molecular dynamics, chlorinated contaminants

INTRODUCTION

Dense non-aqueous phase liquids (DNALPs), such as cis-dichloroethene (cis-DCE) and tetrachloroethene (PCE), pose a significant threat to groundwater resources. Due to their low water solubility and high density, they can readily infiltrate and contaminate aquifers, persisting for extended periods[1,2] since they can sink below the water table and penetrate into groundwater aquifers. Their widespread use in industrial applications, such as cleaning solvents, degreasers, and refrigerants, further exacerbates the problem[3-8]. Remediation of these contaminants is challenging, necessitating the development of efficient technologies. Nanoscale zero-valent iron (nZVI) in the permeable reactive barriers has exhibited considerable potential as a remediation material for removing such chlorinated organic compounds[9-11]. Theoretical studies are still limited in understanding the remediation mechanism of chlorinated organic compounds on nZVI. Zhang *et al.* theoretically investigated the interaction between trichloroethene (TCE) and the Fe(100) surface[12]. They suggested that the chemical adsorption of TCE was a crucial step in its remediation. Later, Lim *et al.* explored the interaction between cis-DCE, PCE, and TCE with the stable flat Fe(110) surface[13,14]. Their results revealed that the removal of the first chlorine exhibited the smallest activation barrier for PCE, followed by TCE and, finally, cis-DCE. This observation also demonstrated that the dissociation of chlorine from contaminants is vital. Additionally, an increase in Cl atoms in the organochlorine molecules led to stronger adsorption on the Fe(110) surface[13,14].

However, nZVI is susceptible to water-induced oxidation and has limited selectivity towards contaminants. To address this challenge, sulfidation of nZVI (S-nZVI) has become an emerging technology that offers improved resistance to water corrosion and a prolonged reactive lifespan[10,15-23]. Our recent investigation into the adsorption of water on S-nZVI revealed that S coverage plays a pivotal role in modifying this interaction[24]. Only the high S coverage can render the surface hydrophobic, leading to weak water adsorption. The S addition can also increase the electron transfer from the nZVI to the contaminants, leading to better remediation of the contaminants[15,23,25-29]. Experimental research has revealed that introducing S produces distinct remediation pathways compared to a pristine nZVI surface[11]. While nZVI has been observed to undergo hydrogenolysis, the S-nZVI has a tendency towards beta-elimination[9,10,29,30]. Consequently, the primary remediation products of organochlorine on the pristine nZVI surface were ethane and ethene, whereas acetylene is the primary production on the S-nZVI[29]. However, Brumovský *et al.* also explored the remediation of cis-DCE, PCE, and TCE on iron sulfide surfaces[16,17]. They found that these organochlorines can only be physically adsorbed on iron sulfide surfaces. These observations underscore the significance of S addition in remediation efforts. However, the previous theoretical study about the remediation of organochlorine contaminant is focused on the sulfidized Fe low index surface. Our previous studies have demonstrated that the high index stepped surface has a higher reactivity due to the surface atoms at the edge of the step having lower coordination numbers (CN)[24,31,32]. Additionally, the stepped surface is abundant in the nanoscale particles. From previous experimental X-ray diffraction (XRD) studies, three mainly exposed facets of nZVI particles are {110}, {200} and {211}[33,34]. The {200} facet has the same structure as the low-indexed (100) surface. Thus, the {211} facet is the main exposed stepped facet in nZVI from the XRD data. Therefore, to comprehensively understand the role of S-nZVI in the wastewater remediation process, it is imperative to investigate the interaction between the contaminant and the sulfidized high index Fe surface, e.g., the (211) surface.

Against this backdrop, this study used the density functional theory (DFT) combined with the ab initio molecular dynamics (AIMD) within the Born-Oppenheimer schemes to elucidate the role of S dopants within S-nZVI for remediating cis-DCE and PCE. We used the Fe(211) surface as a model for comparison with the flat and stable Fe(110) surface. Our theoretical results at the atomic level indicate that the S coverage and the surface morphology are the decisive factors of the remediation performance of S-nZVI.

The findings offer the needed knowledge in guiding the development of tailored S-nZVI materials for efficient degradation of organochlorine contaminants.

METHODS

All DFT computations were performed using the Vienna *Ab initio* Simulation Package (VASP) based on the projector augmented wave (PAW) method with consideration of spin polarization[35,36]. *Vaspkit* was used to build atomic models and post-process the data[37]. The optPBE exchange-correlation energy was employed with the consideration of vdW interaction correction[38-41]. OptPBE was chosen as the method of choice as it has been shown in our previous studies to accurately represent Fe[24,31]. The electron-ion interaction was described using the PAW pseudopotentials, with the $3s^2 3p^6 3d^7 4s^1$, $2s^2 2p^4$, $1s^1$, $3s^2 3p^4$, $3s^2 3p^4$ and $2s^2 2p^2$ treated as valence electrons of Fe, O, H, S, Cl and C, respectively[42]. A plane-wave basis set with a cut-off kinetic energy of 520 eV was used. The gamma-centered k-point meshes with a reciprocal space resolution of $2\pi \times 0.04$ Å^{-1} and $2\pi \times 0.02$ Å^{-1} were utilized for structural optimization and static self-consistent calculations, respectively. The convergence criteria for the self-consistent electronic and structural optimization loop were set to 1×10^{-5} eV and 1×10^{-3} eV/Å, respectively. To represent the solvent effect in the calculations, the implicit solvation model was employed throughout this study using the VASPsol package[43,44].

The (110) and (211) surfaces were modeled using the slab models, separated by a vacuum region of 15 Å to avoid interaction between the surfaces of neighboring slabs along the z-direction. The interlayer distance determined the choice for the number of atomic layers. The (211) surface has a slightly larger interlayer distance with $a_o/\sqrt{6}$; hence, seven atomic layers were used. As a comparison, the interlayer distance of the (110) surface is $a_o/\sqrt{2}$. Thus, only four atomic layers were used. The positions of the atoms in the surface and the adsorbates were allowed to relax.

The adsorption energy for chlorinated organic compounds (ΔE_{CE}) was calculated using:

$$\Delta E_{\mathrm{CE}} = \frac{1}{\mathrm{N}}(E_{Fe/CE} - E_{Fe\_surf} - \mathrm{N}E_{CE})$$

where N is the number of molecules per unit cell. $E_{Fe\text{-}surf}$, $E_{Fe/CE}$ and E_{CE} are the energies of the intrinsic Fe surface, the Fe surface with the adsorbed chlorinated organic compounds, and the chlorinated organic compounds, respectively.

In the AIMD simulations, the (1 × 1 × 1) gamma-centered k-point mesh was applied with a (2 × 2) supercell. Winmostar was used to build the initial configuration of the AIMD calculations[45]. The canonical ensemble (NVT) was used with the Andersen thermostat to simulate the dynamic behavior of the water molecules at 350 K. The simulations were run for 3.5 ps with a time step of 1 fs.

RESULTS AND DISCUSSION

Molecular adsorption

The molecular adsorption of cis-DCE and PCE on pristine Fe(211) and Fe(110) surfaces was first investigated, along with surfaces with low sulfur coverage (termed LC) and high sulfur coverage (termed HC). The optimized cis-DCE molecular adsorption structures are shown in Figure 1. The distances between atoms for all the adsorption sites can be found in the Supplementary Tables 1-16. On the flat pristine (110) surface, the adsorbed cis-DCE is slightly tilted to the surface. Two Cl atoms are adsorbed above the 3-fold hollow site with the adsorption energy of -0.51 eV. Two Cl-Fe bond lengths are 3.46 and 3.16 Å. On the LC

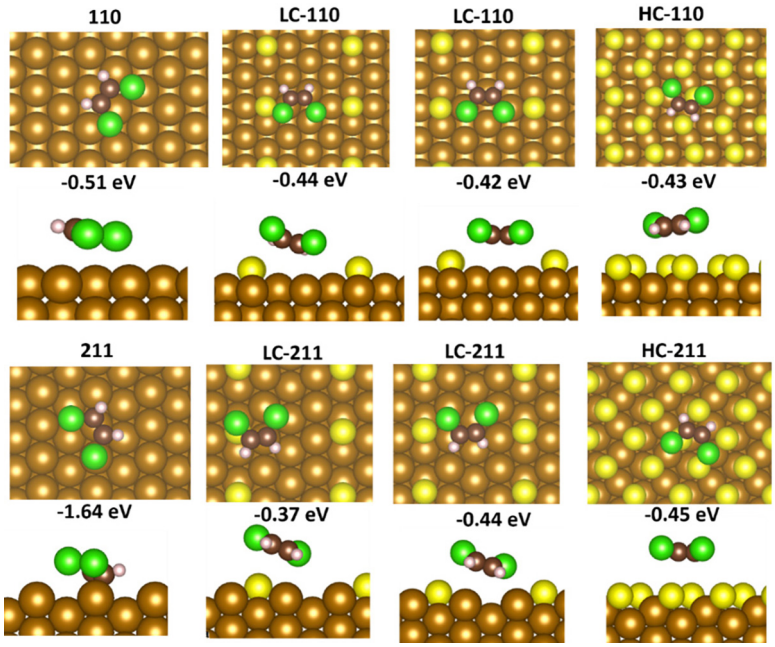

Figure 1. Molecular adsorption of cis-DCE on pristine, low S coverage (LC) and high S coverage (HC) Fe(110) and Fe(211) surfaces (gold: Fe; brown: carbon; green: chlorine; white: hydrogen; yellow: sulfur).

(110) surface, two stable molecular adsorption configurations were identified with relatively weak adsorption strengths of -0.42 and -0.44 eV. When the cis-DCE is close to S, the adsorbed molecule has a more tilted structure, which leads to one shorter Cl-Fe bond length of 3.76 Å and another with a Cl-Fe bond length of 4.62 Å. As a comparison, when the adsorbate is far from the S, the molecular is almost parallel to the surface with a Cl-Fe bond length of 4.02 and 3.93 Å. The shorter Cl-Fe bond length in the tilted configuration when cis-DCE is close to S may be responsible for the slightly lower adsorption energy. At the HC Fe(110), the adsorption energy of cis-DCE is -0.43 eV, which is close to that on the pristine and LC Fe(110) surfaces.

Surprisingly, the molecular adsorption of cis-DCE on the pristine Fe(211) surface is strong with an adsorption energy of -1.64 eV [Figure 1]. This indicates that cis-DCE undertakes a chemisorption spontaneously. It can be ascribed to the specific open stepped surface structure, which enables the direct interaction of C and Cl atoms in cis-DCE with the surface Fe atoms at the edge of the stepped (211) surface, which have the lower CN of 5 in comparison with that on (110) of 6. The two C-Fe bond lengths on Fe(211) are 1.96 and 2.02 Å. The C-Cl bond lengths are 2.40 and 3.26 Å, respectively. Additionally, the C-C bond distance increases from 1.34 to 1.46 Å upon this adsorption, showing the breaking of the double π bonds to form single C-C bonds. It confirms the important influence of surface morphology on the adsorption properties of molecules as we reported before[24,31,32]. After the addition of S both on LC and HC surfaces, the C-Fe interaction is blocked with the corresponding C-Fe bond lengths of 3.62, 3.41, and 4.74 Å for each surface, respectively. As a result, the adsorption energies of cis-DCE are weaker than that on the pristine Fe(211), which are -0.37, -0.44, and -0.45 eV, respectively, as shown in Figure 1. It suggests that the sulfidation has a much larger influence on the stepped surfaces in nZVI for the molecular cis-DCE adsorption.

The optimized molecular PCE adsorption structures on the Fe surfaces are shown in Figure 2. The adsorption energy of PCE on the pristine Fe(110) surface is -0.74 eV, which is about 45% lower than that of the cis-DCE on Fe(110). This agrees with previous studies that the greater number of Cl atoms in the organochlorine molecule can lead to stronger adsorption[13,14]. However, the adsorption energies of PCE on Fe(211) are much weaker than that of the cis-DCE. This may be due to the large size of Cl. The four Cl atoms in PCE effectively prevent the C-Fe interaction, which was observed in the molecular cis-DCE adsorption on pristine Fe(211). In contrast to cis-DCE, PCE exhibits a higher adsorption strength on the pristine Fe(110) surface compared to the Fe(211) surface. This can be ascribed to the great structure match between PCE and the Fe(110) surface, as shown in Figure 2. After the sulfidation at LC and HC, the adsorption of PCE on Fe(110) becomes weaker. On the LC Fe(110) surface, the PCE has an adsorption energy of -0.66 eV when it is far from the S atoms. When the PCE is adsorbed on top of the S, its adsorption energy increases to -0.46 eV. Similar to S-Fe(110) at LC, the PCE adsorption energy increases from -0.65 to -0.56 eV when the adsorbed PCE becomes closer to the surface S on LC Fe(211). However, it is found that three out of the four sites had the same adsorption energy of -0.65 eV on the Fe(211) surfaces. At the high S coverage, the molecular adsorption energies of PCE both on the Fe(110) and (211) are similar, which are -0.62 and -0.65 eV, respectively.

PCE exhibits a greater affinity for Fe surfaces compared to cis-DCE, with the exception of a specific adsorption configuration where cis-DCE is preferentially adsorbed. On the pristine Fe(211) surface, cis-DCE undergoes chemisorption via the formation of chemical bonds with surface Fe atoms. This results in strong adsorption. In contrast, the adsorption of PCE on the same surface is weaker, exhibiting physisorption due to steric constraints imposed by the chlorine atoms.

To further understand the adsorption of the contaminants on the pristine versus sulfur-doped surfaces, Bader charge analysis was undertaken. As present in Supplementary Table 17, the charge transfer upon adsorption onto the clean Fe(211) surface is significant for PCE (+0.14 |e-|). This suggests a strong interaction between the molecule and the surface. A similar trend was observed for low-coverage Fe(110) with PCE adsorbed on sulfur (+0.13 |e-|), indicating favorable interaction with the sulfur atom. However, PCE adsorption on the other low-coverage Fe(110) site resulted in a weaker interaction (+0.07 |e-|). Interestingly, the low-coverage Fe(211) surface exhibited a dependence on the PCE adsorption site. When adsorbed between sulfur atoms, PCE gained a moderate charge (+0.09 |e-|), compared to a minimal transfer (+0.03 |e-|) when positioned directly on top of a sulfur atom. It is also interesting to see that, unlike the Fe(211) surface which had substantial electrons transferred to the PCE, the clean Fe(110) surface exhibited minimal charge transfer to PCE (+0.02 |e-|). Notably, high-coverage Fe(211) displayed no significant charge transfer, while low-level electron transfer (+0.05 |e-|) was observed for high-coverage Fe(110).

For cis-DCE, the Fe(211) surface again facilitated the greatest electron transfer (+0.50 |e-|), consistent with the expected strong chemisorption on this surface. The low-coverage Fe(211) surface with cis-DCE positioned between sulfur atoms also exhibited a considerable charge transfer (+0.23 |e-|). Interestingly, both low-coverage Fe(110) sites displayed similar charge transfer for cis-DCE, regardless of adsorption location on or between sulfur atoms (+0.12 |e-| and +0.13 |e-|, respectively). Finally, for the high-coverage sulfur surfaces, both Fe(211) and Fe(110) resulted in minimal charge transfer to cis-DCE (+0.04 |e-| and +0.02 |e-|, respectively). These observations conclusively demonstrate that both the inherent surface characteristics and the introduction of sulfur atoms significantly impact the charge distribution upon contaminant adsorption.

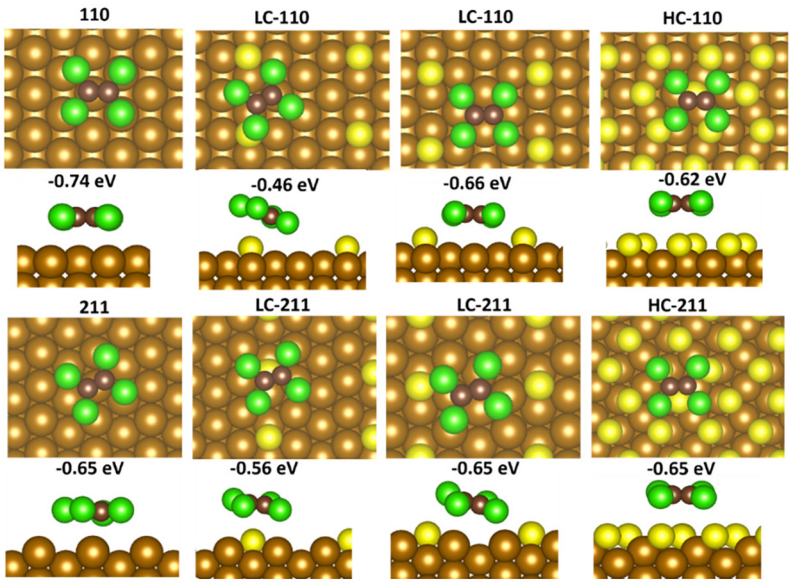

Figure 2. Molecular adsorption of PCE on clean, low sulfur coverage and high sulfur coverage Fe(110) and Fe(211) surfaces (gold: Fe; brown: carbon; green: chlorine; white: hydrogen; yellow: sulfur).

Impact of S coverage and surface morphology

To understand the dynamic feature of the degradation mechanism of cis-DCE and PCE, the AIMD calculations were conducted over a simulation time of 3.5 ps. The calculated energy profiles are shown in Figure 3. The 3.5 ps time scale was chosen because the total energies of all the systems only fluctuate slightly, suggesting that the configurations obtained after 3.5 ps AIMD simulation are thermodynamically stable. On the pristine surfaces, the energy profiles exhibit more pronounced fluctuations, particularly in the initial stages. As a comparison, the total energies have only minor fluctuations over the time period for both cis-DCE and PCE on the HC surfaces. The energy profiles of the two organochlorine molecules on the LC Fe surfaces show a similar trend as that of the pristine surfaces. The energy profiles suggest that the pristine surfaces are the most reactive, which can efficiently trigger chemical adsorption after cis-DCE and PCE are molecularly adsorbed. As a comparison, the HC Fe surface becomes relatively chemically inert, which may not lead to the dissociation of these two contaminants.

Based on the snapshots of the AIMD simulations on the pristine Fe(110) surface with the adsorbed cis-DCE and PCE, both the cis-DCE and PCE undergo activation, leading to the dissociation of the chlorines. The C-C bonds to the Fe surface, with the H atoms initially staying attached to the cis-DCE molecule [Supplementary Figure 1]. During the simulation, one of the H atoms desorbs from the C and binds to the Fe surface. For PCE, one Cl dissociates first and adheres to the Fe surface, allowing the molecule to be vertically and then horizontally adsorbed on the Fe surface [Supplementary Figure 2]. Subsequently, all the Cl atoms dissociate and firmly adsorb onto the Fe(110) surface. In the initial stages of the AIMD simulations on pristine Fe(211) with the adsorbed cis-DCE and PCE, both the cis-DCE and PCE molecules undergo dissociation, with the chlorines adsorbing to the CN5 Fe atoms on the Fe(211) surface. For cis-DCE, the C and H atoms remain bonded together, and both C atoms interact with the CN 5 Fe atoms [Supplementary Figure 3]. For PCE, the initial adsorption of carbon to the CN5 atom leads to the dissociation of two Cl atoms. After that, the third Cl atom dissociated and was adsorbed on the nearby CN5 Fe atom [Supplementary Figure 4]. The last Cl atom appears to be activated, indicating potential dissociation if the simulation were to run longer.

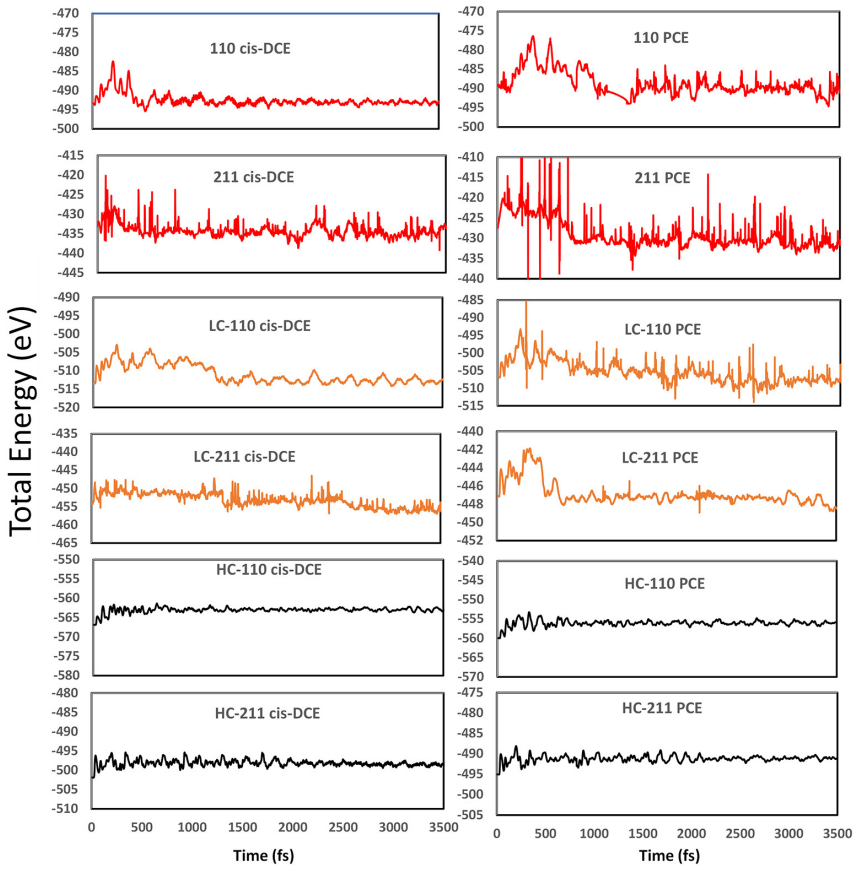

Figure 3. Energy profiles of cis-DCE and PCE on the pristine, S-doped with low S coverage (LC) and S-doped with high S coverage (HC) Fe(110) and (210) surfaces over 3.5 ps.

On the LC Fe(110) surface, both cis-DCE and PCE molecules first undergo distinct configurations [Supplementary Figures 5 and 6]. While the cis-DCE adopts a planar form between the S atoms, the Cl atoms quickly dissociate and bind strongly to the Fe surface. As a result, acetylene was formed and adsorbed on the LC Fe(110) surface. Similarly, the initial steps of the AIMD simulations for PCE involve their movement as a molecular state on the surface. The Cl was then activated by the Fe surfaces to be dissociated, allowing the direct interaction between C in organochlorine and the surface. Thereafter, the second and third Cl atoms dissociate and are shown to be attracted to the sulfur atoms on the surface. The fourth chlorine is shown to still be attached to the carbon, but the bond is elongated to 1.76 Å.

On the LC Fe(211), both the cis-DCE and PCE molecules initially remain in their molecular states for longer before the dissociation, which suggests that sulfur atoms may initially slow the Cl dissociation process, possibly by blocking the interaction between the contaminant and the iron atoms. For cis-DCE, acetylene formed through the dissociation of Cl atoms from cis-DCE can be adsorbed onto the CN5 Fe atoms on the stepped site on the Fe(211) surface [Supplementary Figure 7]. In the case of PCE, the three Cl atoms were dissociated fast in the simulation and bind to the Fe(211) surface. A chloroethylene radical is then adsorbed vertically on the Fe(211) surface [Supplementary Figure 8]. Subsequently, all the Cl atoms bonded to the CN5 Fe atoms, while the C atoms adhered to the stepped site.

Although the dissociation products adsorbed on the pristine and LC Fe surfaces are similar, AIMD simulation results reveal that the dissociation process is different. For both the LC Fe(110) and LC Fe(211) surfaces, the addition of sulfur leads to an easier dissociation of the Cl atoms at later stages, which then gravitate towards the S atoms. On the LC Fe(211) surface, the by-products of acetylene and chloroethylene radical were formed for cis-DCE and PCE, respectively. To this end, both the S coverages and the surface morphology have great influences on the adsorption and degradation of cis-DCE and PCE.

The radial distribution function (RDF) is used to describe the distribution of elements in a system as a function of distance from a reference element. The peak of the RDF indicates a preferred distance between two different elements, while troughs suggest regions with a lower density of the pair of two elements. Figure 4 shows the Cl-Fe RDF images on the pristine, LC, and HC Fe surfaces. The first Fe-Cl distance peaks can be observed at around 2.3 and 2.0 Å on the pristine Fe(110) and Fe(210) surfaces, respectively. On the LC surface, the first peak appears at a slightly larger distance for both contaminants for all but LC-211 cis-DCE. It suggests the introduction of S dopant can have a certain impact on the adsorption at the low S coverage. Following the AIMD simulation on the HC Fe surfaces, no dissociation products were observed. Consequently, a significant spatial gap between the Fe atoms and chlorines is depicted in the RDF, highlighting the absence of dissociation products in this scenario. This suggests that high sulfur coverage can hinder the dissociation of cis-DCE and PCE greatly.

To further understand the properties of the final product with the different S coverage on the flat (110) and stepped (211) surfaces, the surface structures of the adsorbed organochlorine obtained from the final structure of the AIMD simulations were optimized using DFT to understand the adsorption properties of cis-DCE and PCE on clean, LC and HC Fe(110) and Fe(211) surfaces. Figure 5 shows the adsorption properties of cis-DCE and PCE on the pristine, LC, and HC Fe(110) surfaces. The distances for all dissociated systems are found in the Supplementary Tables 18-28. Both contaminants were dissociated on the pristine and LC Fe(110) surface with the adsorption energies about ten times lower than that of the molecular adsorption. Both the Cl atoms and one H atom dissociated when cis-DCE was dissociated on pristine Fe(110), while the C-C bond remained. The chlorine atoms and the dissociated H atom were adsorbed onto the hollow sites. Interestingly, the acetylene was observed after the dissociation of cis-DCE on LC Fe(110), which matches the experimental observation reported by Brumovský *et al.* that the acetylene is the primary product on the S-nZVI[29]. As a comparison, the cis-DCE keeps the molecular state on the HC Fe(110) surface, which agrees with the study by Brumovský *et al.*[16] that the organochlorines can only be physically adsorbed on iron sulfide surfaces[24,31,32]. A similar trend was also identified when the PCE was adsorbed on the pristine, LC and HC Fe(110) surface. Due to the strong Fe-Cl interactions, the adsorption energies of dissociative PCE on the pristine and LC Fe(110) surface are lower than that of the cis-DCE. On the HC Fe(110) surface, the adsorption energy of the cis-DCE is close to its molecular adsorption energy. As a comparison, the adsorption energy of PCE is 0.21 eV higher than its molecular adsorption energy. This may be ascribed to the high mobility of PCE on the HC surface due to the weak adsorption. As a result, the initial structure from the AIMD simulation shifts from the global minimum point.

The adsorption properties of both contaminants on the pristine, LC and HC Fe(211) surfaces are depicted in Figure 6, demonstrating a similar trend to that observed on Fe(110). Both contaminants were dissociated on the pristine and LC surfaces. Again, the acetylene was observed after the dissociation of cis-DCE on LC Fe(110), which matches the experimental observation[29]. The adsorption energy of the dissociated PCE is lower than that of the dissociated cis-DCE. On the HC Fe surfaces, PCE adsorbed molecularly. This is in agreement with Brumovský *et al.*, who reported only molecular adsorption occurred on FeS(001) with -0.63 eV for PCE[16]. On Fe(211), the C and Cl atoms were adsorbed onto the Fe atoms at the edge of the

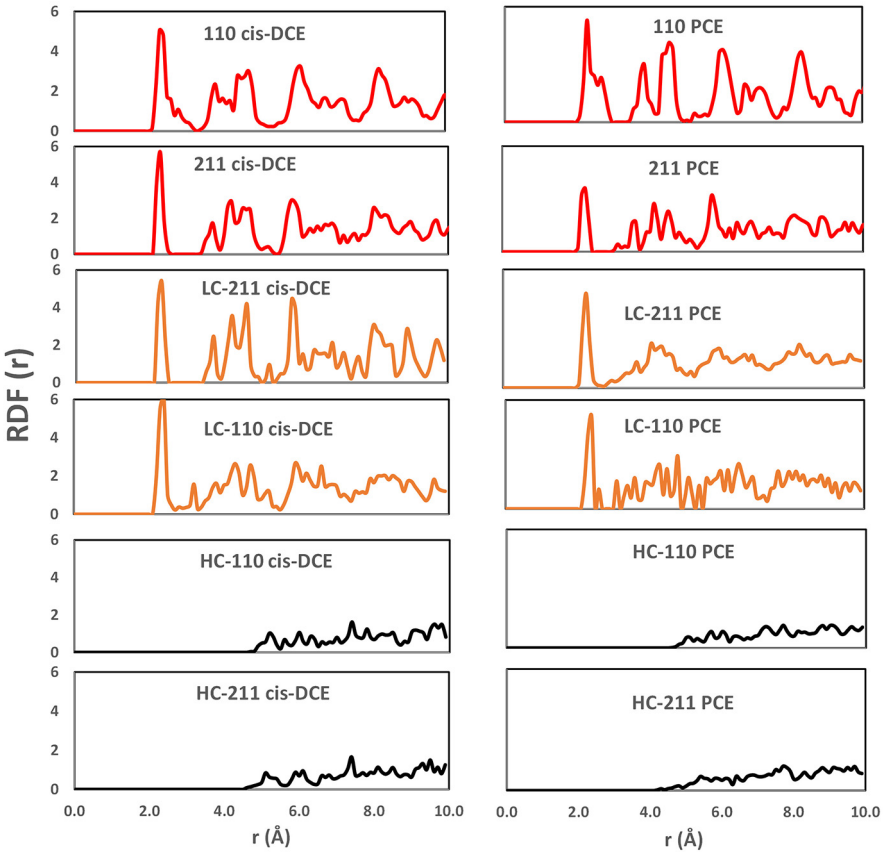

Figure 4. Radial distribution function between the iron and chlorine atoms on the pristine (red), LC (orange) and HC (black) Fe(110) and Fe(211) surfaces.

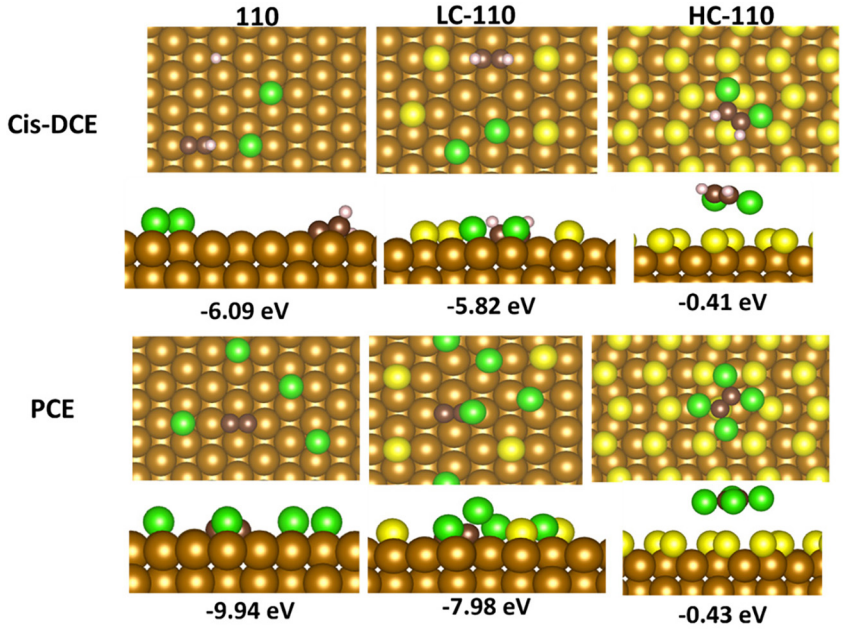

Figure 5. Optimized adsorption structures of cis-DCE and PCE on the pristine, LC and HC Fe(110) along with the corresponding adsorption energies (gold: Fe; brown: carbon; green: chlorine; white: hydrogen; yellow: sulfur).

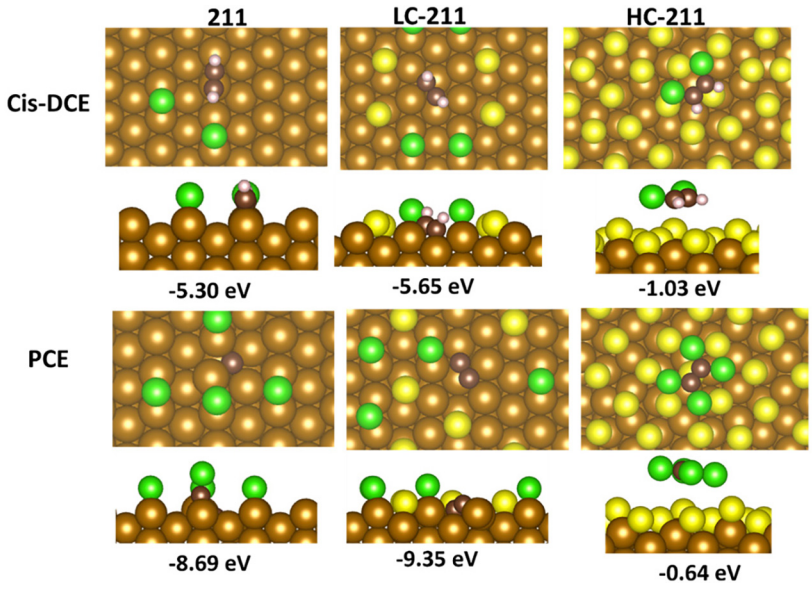

Figure 6. Optimized adsorption structures of cis-DCE and PCE on the pristine, LC and HC Fe(211) along with the corresponding adsorption energies (gold: Fe; brown: carbon; green: chlorine; white: hydrogen; yellow: sulfur).

stepped surface with the lowest CN of 5. For the PCE, the C-C bond broke with one chlorine adsorbing on the side of the step, while the other carbon remained connected to one chlorine and adsorbed on top of the CN5 Fe atom. The other chlorine atoms were adsorbed on the bridge site of the Fe(211) surface. Additionally, the molecular adsorption energies of cis-DCE and PCE are -1.03 eV for and -0.64 eV, respectively, on the HC Fe(211) surface. The higher adsorption energy of cis-DCE compared to its molecular adsorption can still be ascribed to high mobility of cis-DCE on the HC surface due to the weak adsorption. As a result, the initial structure from the AIMD simulation shifts from the global minimum point.

Furthermore, the adsorption energies of both contaminants on HC Fe(210) are much lower than those on the HC Fe(110) surface. The different structural and energetic properties of both contaminants on Fe(110) and (210) suggest that the stepped surface in nZVI is more reactive for removing the organochlorine. This agrees with our previous studies that the surface Fe atoms have higher reactivity due to their lower CN[24,31,32]. Our AIMD results further propose that the S atoms on the stepped surface may still have a higher reactivity toward the physical adsorption of the organochlorine contaminants. To further understand the role of the S dopants on the stepped surface, the Partial Density of States (PDOS) of the Cl atom in cis-DCE or PCE and their closest S atoms both in HC Fe(110) and Fe(210) surfaces were analyzed along with the PDOS of the Cl atom in the molecularly adsorbed contaminants on the pristine surface, which are shown in Figure 7. On the HC surface, the peaks of Cl states in the bonding energy move towards the lower energy level. One example of this state shift can be found in the dash lines in Figure 7. This band shift towards the lower energy level suggests that the surface S can have considerable interaction with the molecular contaminants. Especially, the shift is stronger when S is on the HC Fe(211) surface, which indicates that the S on the HC Fe(211) surface is more reactive than that on the HC Fe(110) surface. The high reactivity of S on HC Fe(211) can further be demonstrated by the stronger overlap between the Cl and S states at the range between [-7, -5] for cis-DCE and [-6, -4] for the PCE on the HC Fe(211) surface.

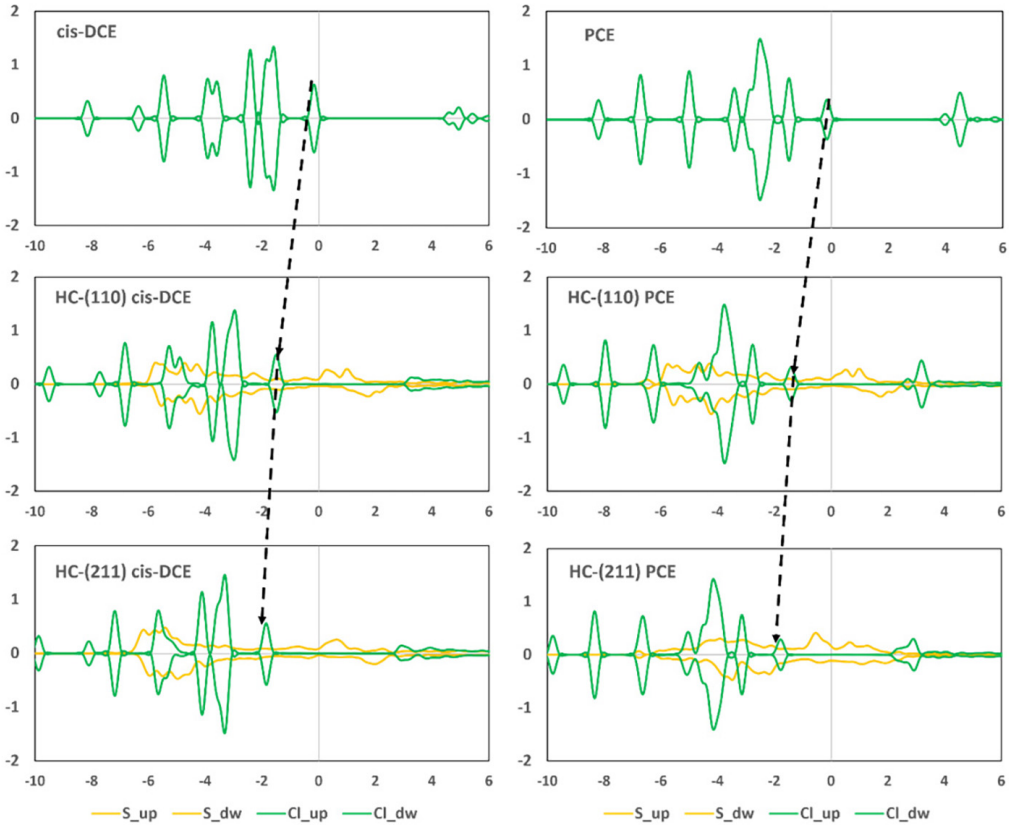

Figure 7. Partial Density of States (PDOS) of S p and Cl p orbitals on the HC Fe(110) and Fe(211). The Cl p orbitals of the unabsorbed contaminant was added for comparison to the adsorbed states (green: chlorine; orange: sulfur).

Competitive adsorption of water

As the main benefit of S-nZVI is its increased selectivity towards contaminants, we investigate the selectivity through the comparison of the molecular adsorption properties between water and two contaminants on the pristine, LC and HC Fe(110) and Fe(211) surfaces. The water adsorption properties on the sulfidized surfaces have been studied with the inclusion of the solvation effect [Supplementary Figure 9]. In Figure 8, the adsorption selectivity towards cis-DCE and PCE was quantified. Using the molecular water adsorption energy as the reference of 0, the positive values shown in Figure 8 suggest a higher selectivity toward the contaminant adsorption. The corresponding adsorption energies are listed in Supplementary Table 29. On the pristine (110) surface, the cis-DCE exhibits weaker adsorption in comparison with the water adsorption. On the pristine (211) surface, cis-DCE has a strong adsorption with -1.64 eV compared to molecular water adsorption with -0.70 eV. As a result, the cis-DCE can be highly selectively adsorbed on the stepped surface. However, the adsorption of PCE on the pristine (211) surface is weaker than that of water molecules. To this end, the selectivity of the adsorption of the contaminants is largely determined by the surface morphology and the contaminants species. On the LC surfaces, cis-DCE adsorption cannot compete with that of water when the adsorbed cis-DCE are far from the surface S and directly interact with the surface S atoms. However, the adsorption of cis-DCE will become highly selective when the cis-DCE is adsorbed on S atoms. Meanwhile, the PCE has a stronger adsorption on all LC Fe surfaces. As the S coverage further increases, the adsorption of cis-DCE and PCE becomes dominant on all HC Fe surfaces. These results demonstrate that increased S coverage can significantly improve the selectivity of the contaminant adsorption on both the flat and stepped surfaces with the nZVI.

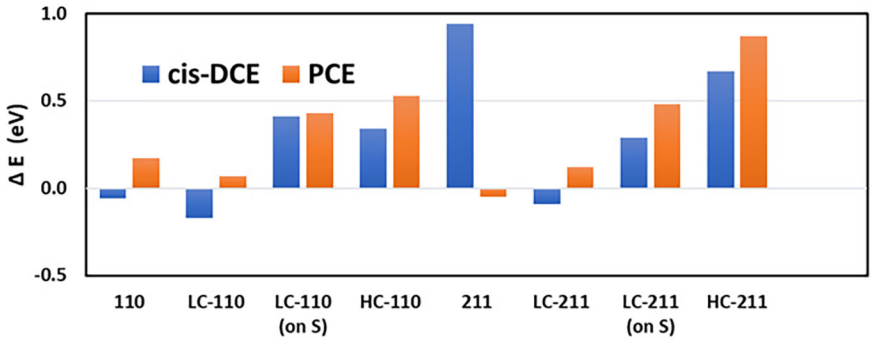

Figure 8. The energy differences (ΔE) between water and contaminant adsorption by using the water adsorption energy as the reference of 0 eV. The positive energy difference indicates a higher selectivity towards the contaminant adsorption (blue: cis-DCE; orange: PCE).

CONCLUSIONS

In this study, we used cis-DCE and PCE as the model organochlorine contaminants to theoretically investigate the impact of the S coverage and the surface morphology of the S-nZVI on their remediation performance. First, the sulfidation of Fe(110) and Fe(211) can increase selectivity towards cis-DCE and PCE. To this end, S-nZVI can remediate these contaminants more successfully. Our DFT and AIMD results successfully explained the reported experimental observations. For example, the acetylene product can only be formed on the LC Fe surface, which is in agreement with the beta-elimination mechanism shown in experimental studies[27]. As a comparison, the organochlorine cannot be efficiently dissociated when the S coverage is high, as observed on the iron sulfide surfaces[16,17]. Thus, the high S coverage can only benefit the remediation of organochlorine contaminants through the adsorption mechanism. However, moderate S coverage is required to degrade the organochlorine molecules if they are to be decomposed and reduced by surface Fe atoms on nZVI. This study provides valuable theoretical insights into the interplay between S doping and nZVI surface characteristics, guiding the development of optimized S-nZVI materials for efficient and targeted remediation of chlorinated organic contaminants in wastewater treatment applications.

DECLARATIONS

Acknowledgments

This research was undertaken on the supercomputers in the National Computational Infrastructure (NCI) in Canberra, Australia, which is supported by the Australian Commonwealth Government and Pawsey Supercomputing Center in Perth, with funding from the Australian Government and the Government of Western Australia.

Authors' contributions

Methodology, software, formal analysis, writing - original draft: White JJ
Writing - review & editing: Zhou M, Hinsch JJ, Bennett WW
Project administration, funding acquisition, supervision, conceptualization, methodology, resources: Wang Y

Availability of data and materials

The data that support the findings of this study are available from the corresponding author upon reasonable request.

Financial support and sponsorship
This work was supported by the Australian Research Council Discovery Project (Grant No. DP210103266).

Conflicts of interest
All authors declared that there are no conflicts of interest.

Ethical approval and consent to participate
Not applicable.

Consent for publication
Not applicable.

REFERENCES

1. Fagerlund F, Illangasekare TH, Phenrat T, Kim HJ, Lowry GV. PCE dissolution and simultaneous dechlorination by nanoscale zero-valent iron particles in a DNAPL source zone. *J Contam Hydrol* 2012;131:9-28. DOI
2. Qian L, Chen Y, Ouyang D, et al. Field demonstration of enhanced removal of chlorinated solvents in groundwater using biochar-supported nanoscale zero-valent iron. *Sci Total Environ* 2020;698:134215. DOI
3. Lien HL, Zhang WX. Hydrodechlorination of chlorinated ethanes by nanoscale Pd/Fe bimetallic particles. *J Environ Eng* 2005;131:4-10. DOI
4. Lin KS, Mdlovu NV, Chen CY, Chiang CL, Dehvari K. Degradation of TCE, PCE, and 1,2-DCE DNAPLs in contaminated groundwater using polyethylenimine-modified zero-valent iron nanoparticles. *J Clean Prod* 2018;175:456-66. DOI
5. Xu W, Li Z, Shi S, et al. Carboxymethyl cellulose stabilized and sulfidated nanoscale zero-valent iron: characterization and trichloroethene dechlorination. *Appl Catal B Environ* 2020;262:118303. DOI
6. Huang J, Yi S, Zheng C, Lo IMC. Persulfate activation by natural zeolite supported nanoscale zero-valent iron for trichloroethylene degradation in groundwater. *Sci Total Environ* 2019;684:351-9. DOI
7. Gu M, Farooq U, Lu S, Zhang X, Qiu Z, Sui Q. Degradation of trichloroethylene in aqueous solution by rGO supported nZVI catalyst under several oxic environments. *J Hazard Mater* 2018;349:35-44. DOI PubMed
8. Idrees A, Shan A, Ali M, et al. Highly efficient degradation of trichloroethylene in groundwater based on persulfate activation by polyvinylpyrrolidone functionalized Fe/Cu bimetallic nanoparticles. *J Environ Chem Eng* 2021;9:105341. DOI
9. Bhattacharjee S, Ghoshal S. Optimal design of sulfidated nanoscale zerovalent iron for enhanced trichloroethene degradation. *Environ Sci Technol* 2018;52:11078-86. DOI PubMed
10. He F, Li Z, Shi S, et al. Dechlorination of excess trichloroethene by bimetallic and sulfidated nanoscale zero-valent iron. *Environ Sci Technol* 2018;52:8627-37. DOI
11. Mo Y, Xu J, Zhu L. Molecular structure and sulfur content affect reductive dechlorination of chlorinated ethenes by sulfidized nanoscale zerovalent iron. *Environ Sci Technol* 2022;56:5808-19. DOI
12. Zhang N, Luo J, Blowers P, Farrell J. Understanding trichloroethylene chemisorption to iron surfaces using density functional theory. *Environ Sci Technol* 2008;42:2015-20. DOI PubMed PMC
13. Lim DH, Lastoskie CM, Soon A, Becker U. Density functional theory studies of chloroethene adsorption on zerovalent iron. *Environ Sci Technol* 2009;43:1192-8. DOI PubMed
14. Lim DH, Lastoskie CM. Density functional theory studies on the relative reactivity of chloroethenes on zerovalent iron. *Environ Sci Technol* 2009;43:5443-8. DOI PubMed
15. Bin Q, Lin B, Zhu K, et al. Superior trichloroethylene removal from water by sulfide-modified nanoscale zero-valent iron/graphene aerogel composite. *J Environ Sci* 2020;88:90-102. DOI
16. Brumovský M, Micić V, Oborná J, Filip J, Hofmann T, Tunega D. Iron nitride nanoparticles for rapid dechlorination of mixed chlorinated ethene contamination. *J Hazard Mater* 2023;442:129988. DOI PubMed
17. Brumovský M, Oborná J, Micić V, et al. Iron nitride nanoparticles for enhanced reductive dechlorination of trichloroethylene. *Environ Sci Technol* 2022;56:4425-36. DOI PubMed PMC
18. Cao Z, Li H, Lowry GV, et al. Unveiling the role of sulfur in rapid defluorination of florfenicol by sulfidized nanoscale zero-valent iron in water under ambient conditions. *Environ Sci Technol* 2021;55:2628-38. DOI
19. Chen J, Dong H, Tian R, Li R, Xie Q. Remediation of trichloroethylene-contaminated groundwater by sulfide-modified nanoscale zero-valent iron supported on biochar: investigation of critical factors. *Water Air Soil Pollut* 2020;231:4797. DOI
20. Fan D, O'Brien Johnson G, Tratnyek PG, Johnson RL. Sulfidation of nano zerovalent iron (nZVI) for improved selectivity during in-situ chemical reduction (ISCR). *Environ Sci Technol* 2016;50:9558-65. DOI PubMed

21. Li X, Zeng L, Wen N, Deng D. Critical roles of sulfidation solvent in controlling surface properties and the dechlorination reactivity of S-nZVI. *J Hazard Mater* 2021;417:126014. DOI PubMed
22. Wang B, Dong H, Li L, et al. Influence of different co-contaminants on trichloroethylene removal by sulfide-modified nanoscale zero-valent iron. *Chem Eng J* 2020;381:122773. DOI
23. Zhan J, Ma M, Zhang X, et al. Comparison of trichloroethylene dechlorination in seawater by sulfidated nanoscale zero-valent iron particles prepared by two methods. *J Environ Chem Eng* 2023;11:110242. DOI
24. White JJ, Hinsch JJ, Wu Z, Tian Y, Bennett WW, Wang Y. Sulfidation impacts on the hydrophobicity of stepped iron surfaces. *Adv Energy Sustain Res* 2023;4:2300055. DOI
25. Cao Z, Li H, Xu X, Xu J. Correlating surface chemistry and hydrophobicity of sulfidized nanoscale zerovalent iron with its reactivity and selectivity for denitration and dechlorination. *Chem Eng J* 2020;394:124876. DOI
26. Dong H, Zhang C, Deng J, et al. Factors influencing degradation of trichloroethylene by sulfide-modified nanoscale zero-valent iron in aqueous solution. *Water Res* 2018;135:1-10. DOI
27. Garcia AN, Zhang Y, Ghoshal S, He F, O'Carroll DM. Recent advances in sulfidated zerovalent iron for contaminant transformation. *Environ Sci Technol* 2021;55:8464-83. DOI PubMed
28. Xu J, Cao Z, Zhou H, et al. Sulfur dose and sulfidation time affect reactivity and selectivity of post-sulfidized nanoscale zerovalent iron. *Environ Sci Technol* 2019;53:13344-52. DOI
29. Brumovský M, Filip J, Malina O, et al. Core-shell Fe/FeS nanoparticles with controlled shell thickness for enhanced trichloroethylene removal. *ACS Appl Mater Interfaces* 2020;12:35424-34. DOI PubMed PMC
30. Xu J, Wang Y, Weng C, et al. Reactivity, selectivity, and long-term performance of sulfidized nanoscale zerovalent iron with different properties. *Environ Sci Technol* 2019;53:5936-45. DOI
31. White JJ, Hinsch JJ, Bennett WW, Wang Y. Theoretical understanding of water adsorption on stepped iron surfaces. *Appl Surf Sci* 2022;605:154650. DOI
32. White JJ, Liu J, Hinsch JJ, Wang Y. Theoretical understanding of the properties of stepped iron surfaces with van der Waals interaction corrections. *Phys Chem Chem Phys* 2021;23:2649-57. DOI
33. Xu J, Li H, Lowry GV. Sulfidized nanoscale zero-valent iron: tuning the properties of this complex material for efficient groundwater remediation. *ACC Mater Res* 2021;2:420-31. DOI
34. Xu J, Avellan A, Li H, et al. Sulfur loading and speciation control the hydrophobicity, electron transfer, reactivity, and selectivity of sulfidized nanoscale zerovalent iron. *Adv Mater* 2020;32:e1906910. DOI
35. Kresse G, Hafner J. Ab initio molecular dynamics for liquid metals. *Phys Rev B Condens Matter* 1993;47:558-61. DOI PubMed
36. Kresse G, Furthmüller J. Efficiency of *ab-initio* total energy calculations for metals and semiconductors using a plane-wave basis set. *Comput Mater Sci* 1996;6:15-50. DOI
37. Wang V, Xu N, Liu J, Tang G, Geng W. VASPKIT: a user-friendly interface facilitating high-throughput computing and analysis using VASP code. *Comput Phys Commun* 2021;267:108033. DOI
38. Dion M, Rydberg H, Schröder E, Langreth DC, Lundqvist BI. van der Waals density functional for general geometries. *Phys Rev Lett* 2004;92:246401. DOI
39. Thonhauser T, Cooper VR, Li S, Puzder A, Hyldgaard P, Langreth DC. Van der Waals density functional: self-consistent potential and the nature of the van der Waals bond. *Phys Rev B* 2007;76:125112. DOI
40. Klimeš J, Bowler DR, Michaelides A. Van der Waals density functionals applied to solids. *Phys Rev B* 2011;83:195131. DOI
41. Lee K, Murray ÉD, Kong L, Lundqvist BI, Langreth DC. Higher-accuracy van der Waals density functional. *Phys Rev B* 2010;82:081101. DOI
42. Kresse G, Joubert D. From ultrasoft pseudopotentials to the projector augmented-wave method. *Phys Rev B* 1999;59:1758-75. DOI
43. Mathew K, Sundararaman R, Letchworth-Weaver K, Arias TA, Hennig RG. Implicit solvation model for density-functional study of nanocrystal surfaces and reaction pathways. *J Chem Phys* 2014;140:084106. DOI PubMed
44. Mathew K, Kolluru VSC, Mula S, Steinmann SN, Hennig RG. Implicit self-consistent electrolyte model in plane-wave density-functional theory. *J Chem Phys* 2019;151:234101. DOI PubMed
45. Martínez L, Andrade R, Birgin EG, Martínez JM. PACKMOL: a package for building initial configurations for molecular dynamics simulations. *J Comput Chem* 2009;30:2157-64. DOI PubMed